催化学报
2012 Chinese Journal of Catalysis Vol. 33 No. 7

文章编号: 0253-9837(2012)07-1101-08 国际版 DOI: 10.1016/S1872-2067(11)60382-3 研究论文: 1101~1108

可分散的 In_2O_3/Ta_2O_5 复合光催化剂的制备及其光催化制氢性能

许蕾蕾, 倪 磊, 施伟东, 官建国*

武汉理工大学材料复合新技术国家重点实验室, 湖北武汉 430070

摘要: 通过控制乙醇钽的水解速率, 在丙酮水溶液中制备了可分散的 Ta_2O_5 微球, 并以此为载体构建了 In_2O_3/Ta_2O_5 异质结复合光催化剂, 利用扫描电子显微镜、X 射线能量色散光谱、粉末 X 射线衍射光谱、透射电子显微镜和紫外-可见漫反射光谱等手段对样品形貌、结构和光吸收性质进行了表征. 结果表明, In_2O_3 纳米粒子分布在 Ta_2O_5 微球表面, 且两相间存在明显的界面, 同时 In_2O_3 的复合拓宽了 Ta_2O_5 的光吸收范围, 有利于光生电子与空穴的分离, 使复合光催化剂在模拟太阳光照射下表现出更高的光解水制氢活性.

关键词: 可分散微球; 五氧化二钽; 三氧化二铟; 异质结构; 光催化; 产氢

中图分类号: O643 **文献标识码**: A

收稿日期: 2012-01-17. 接受日期: 2012-02-28.

*通讯联系人. 电话: (027)87218832; 传真: (027)87879468; 电子信箱: guanjg@whut.edu.cn

基金来源: 国家自然科学基金 (51002111, 21001086); 中国博士后科学基金 (20100471163, 201104494); 湖北省自然科学基金 (2010CDA030, 2010CDB00606); 武汉市学科带头人计划 (201150530145).

本文的英文电子版(国际版)由Elsevier出版社在ScienceDirect上出版(http://www.sciencedirect.com/science/journal/18722067).

Photocatalytic Activity for Hydrogen Evolution over Well-Dispersed Heterostructured In_2O_3/Ta_2O_5 Composites

XU Leilei, NI Lei, SHI Weidong, GUAN Jianguo*

State Key Laboratory of Advanced Technology for Materials Synthesis and Processing, Wuhan University of Technology, Wuhan 430070, Hubei, China

Abstract: Using well-dispersed Ta_2O_5 microspheres as supports, which were prepared by controlling the hydrolysis rates of tantalum ethoxide via the formation of glycolate in an acetone-water mixture, dispersible heterostructured In_2O_3/Ta_2O_5 composites were fabricated for photocatalytic hydrogen evolution under simulant solar light irradiation. The compositions, structure, morphologies, and optical absorption properties of these composites were characterized using scanning electron microscopy, energy-dispersive X-ray spectroscopy, X-ray diffraction, transmission electron microscopy, and UV-Vis diffuse reflectance spectroscopy. The results show that in the as-prepared heterostructured In_2O_3/Ta_2O_5 composites, In_2O_3 nanoparticles are well distributed on the surface of Ta_2O_5 microspheres with a clear interface between the two phases. The incorporation of In_2O_3 extends the light absorption range and restricts photogenerated charge-carrier recombination, resulting in enhanced photocatalytic activity for hydrogen evolution.

Key words: well-dispersed microsphere; tantalum pentoxide; indium trioxide; heterostructure; photocatalysis; hydrogen production

Received 17 January 2012. Accepted 28 February 2012.

**Corresponding author. Tel: +86-27-87218832; Fax: +86-27-87879468; E-mail: guanjg@whut.edu.cn*

This work was supported by the National Natural Science Foundation of China (51002111 and 21001086), the China Postdoctoral Science Foundation (20100471163 and 201104494), the Natural Science Foundation of Hubei Province (2010CDA030 and 2010CDB00606), and the Subject Leadership Project of Wuhan City (201150530145).

English edition available online at Elsevier ScienceDirect (http://www.sciencedirect.com/science/journal/18722067).

光催化制氢可以将太阳能转化为可直接利用的化学能, 被誉为最理想的新能源开发手段之一[1~4]. 钽基材料独特共顶角八面体 (TaO_6) 结构有利于光催化过程中光生电子与空穴的迁移, 且 Ta 5*d* 轨道

构成的导带比 Ti 3*d* 轨道更负, 使得其上电子的还原能力更强[5,6]. 因此, 钽基材料在光催化制氢领域表现出潜在的应用前景. 然而, 紫外光活化与助催化剂辅助制约了此类材料的实际应用[7,8]. 相比于离子掺杂和染料敏化等改性方法, 构建异质结复合半导体能在拓宽宽禁带半导体光响应范围的同时, 实现光生电子与空穴的有效分离, 因而引起了人们的广泛关注. 目前制备的异质结复合半导体多数为两种半导体颗粒的随机混合物, 如 Pt/PdS/CdS[9], MoS_2/CdS[10], ZnO/CdS[11] 和 ZnO/In_2O_3[12] 等, 通常存在异质结有效面积较小, 光致电荷被分离后要经过复杂的途径才能传递到表面, 以及采光和传质效率不高等缺点, 因而极大地降低了异质结的作用. 因此异质结复合半导体构型的设计对提高光催化制氢效率具有十分重要的意义.

本文先以乙醇钽和乙醇酸盐为前驱体, 制备分散性较好的 Ta_2O_5 微球, 再以此为载体, 构建 In_2O_3/Ta_2O_5 异质结复合材料并用于模拟太阳光催化制氢的反应中, 考察 In_2O_3 含量对复合材料光吸收性质及模拟太阳光催化制氢活性的影响, 分析光生载流子分离机理.

1 实验部分

1.1 催化剂的制备

在真空手套箱中, 将 0.4 g $Ta(OC_2H_5)_5$ 溶于 10 ml 乙二醇中, 于室温搅拌 8 h 得澄清透明溶液. 将上述混合溶液移出手套箱后迅速灌注到 100 ml 含 0.5 vol% 水的丙酮中, 高速搅拌 10 min, 静置 30 min 后分离, 并分别水洗醇洗三次, 于 60 ºC 干燥 24 h, 即得 Ta_2O_5 微球.

称取 0.22 g 制得的 Ta_2O_5 微球分散于 50 ml 水中, 超声 10 min 使其均匀分散. 然后于室温搅拌下加入一定量的 $In(NO_3)_3{\cdot}nH_2O$, 并使其溶解完全, 再加入氨水, 控制溶液 pH 值大于 9, 得到白色沉淀. 最后离心分离出样品, 并分别水洗和醇洗各三次, 以除去表面吸附的杂质, 再于 60 ºC 干燥 24 h, 800 ºC 退火 2 h 后得到白色粉末状固体 In_2O_3/Ta_2O_5.

1.2 催化剂的表征

样品的扫描电镜 (SEM) 观察在日本日立公司 Hitachi S-4800 型场发射扫描电镜上进行. 能谱 (EDX) 检测采用日本日立公司 Horbia EX-250 型能谱仪. 样品的晶体结构采用日本理学 D/max-RB 型全自动转靶 X 射线衍射 (XRD) 分析仪进行测试, Cu K_α 靶线 (λ = 0.10154 nm), 加速电压 15 kV, 电流 20 mA, 扫描速率 0.05º/s. 样品的透射电镜 (TEM) 和高分辨透射电镜 (HRTEM) 表征采用日本日立公司 H-600 STEM/EDX PV9100 型透射电子显微镜. 样品的紫外-可见漫反射光谱 (UV-Vis DRS) 采用日本岛津 UV-2550 型紫外-可见分光光度计进行测试.

1.3 光催化反应

模拟太阳光催化制氢反应在装有取样阀, 且与气相色谱连接的 LabSolar H_2 光解水制氢封闭循环体系中进行. 模拟太阳光源为配有红外滤光片的 PLS-SXE 300 型氙灯 (功率为 300 W, 发射光波长为 320~780 nm), 可见光源为配有 UV-cut 滤光片的 PLS-SXE 300 型氙灯. 将 150 mg 催化剂与约 3.15 mg 的氯铂酸 (质量百分数约为 1%) 加入到含 80 ml 去离子水和 20 ml 甲醇的石英玻璃反应器中, 并磁力搅拌使催化剂均匀悬浮, 把反应器与系统连接起来. 采用原位光还原进行 Pt 的负载[13,14], 光照前, 将体系在搅拌状态下反复进行数次抽真空至–0.1 MPa, 以去除系统中的溶解氧及其它气体. 抽真空完毕后, 将真空泵和系统断开, 开始光照, 反应每隔一段时间取样, 在气相色谱仪 (GC 7890II, 上海天美科学仪器有限公司) 上进行在线分析, 5A 分子筛填充柱, 柱温 45 ºC, 载气 N_2, 进样温度为 120 ºC; TCD 检测器, 温度 120 ºC, 桥流 100 mA.

2 结果与讨论

2.1 In_2O_3/Ta_2O_5 的结构和形貌

图 1 为不同 In_2O_3 含量的 In_2O_3/Ta_2O_5 复合催化剂的 SEM 照片和 EDX 谱. 可以看出, 复合材料中 Ta_2O_5 微球仍维持其原有形貌, 粒径约为 240 nm. 退火后的微球表面较粗糙, 且缺陷增多. 引入的 In 主要以纳米粒子的形式存在于载体表面, 且随着 In 含量的增加而出现 In 的团聚态. 由相应的 EDX 谱可知, 复合材料主要由 Ta, O 和 In 元素组成.

图 2 为不同 In_2O_3 含量的 In_2O_3/Ta_2O_5 复合催化剂的 XRD 谱. 可以看出, Ta_2O_5 在 2θ = 23.1º, 29.2º, 37.8º, 47.3º, 51.2º 以及 56.8º 处出现正交晶相 Ta_2O_5 的特征衍射峰 (JCPDS 79-1375). 随着催化剂中 In_2O_3 摩尔百分含量增至 20%, 在 2θ = 30.6º 和 35.5º

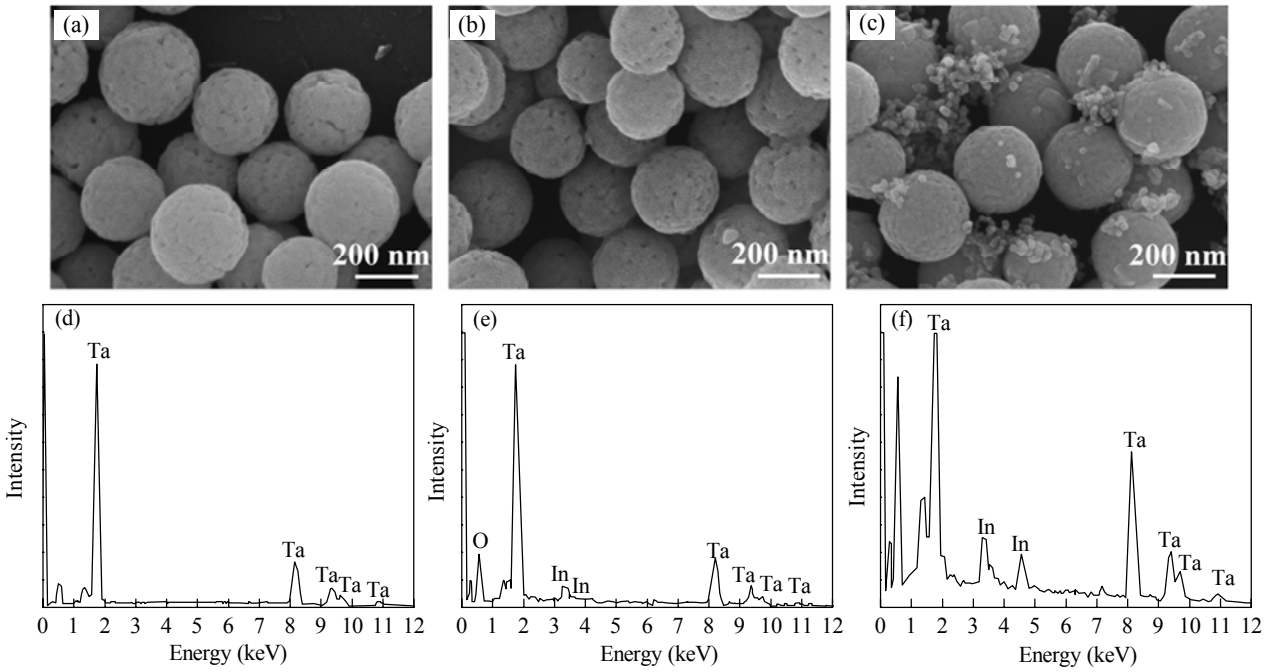

图 1 不同 In_2O_3 含量的 In_2O_3/Ta_2O_5 复合催化剂的 SEM 照片和 EDX 谱

Fig. 1. SEM images (a–c) and EDX profiles (d–f) of the as-prepared In_2O_3/Ta_2O_5 composites with different In_2O_3 mole percents. (a,d) 0; (b,e) 5%; (c,f) 20%.

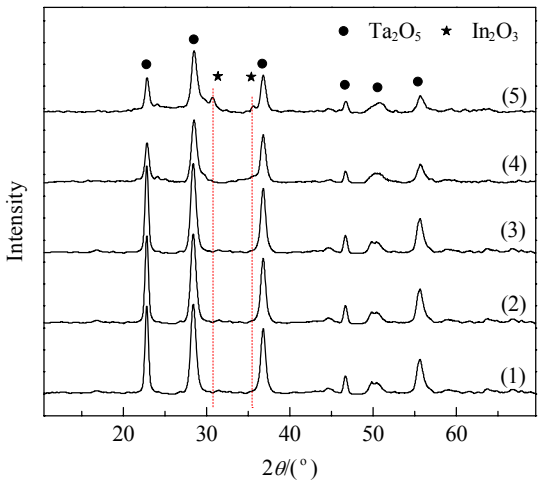

图 2 不同 In_2O_3 含量的 In_2O_3/Ta_2O_5 复合催化剂的 XRD 谱

Fig. 2. XRD patterns of In_2O_3/Ta_2O_5 composites with different In_2O_3 mole percents. (1) 0; (2) 2%; (3) 5%; (4) 10%; (5) 20%.

出现立方晶相 In_2O_3 的特征衍射峰 (JCPDS 71-2194), 说明在复合材料中, In 主要以 In_2O_3 的形式存在, 另外, 随着 In_2O_3 含量的增加, 样品中 Ta_2O_5 的衍射峰强度逐渐降低, 说明 In_2O_3 的加入在一定程度上影响了 Ta_2O_5 的结晶度.

图 3 为 5%In_2O_3/Ta_2O_5 复合催化剂的 TEM 和 HRTEM 照片. 可以看出, 可分散的 Ta_2O_5 微球粒径

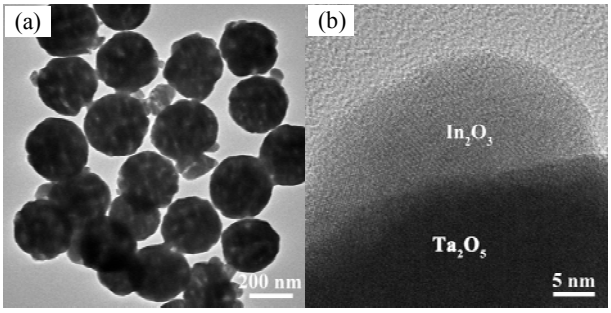

图 3 5%In_2O_3/Ta_2O_5 复合催化剂的 TEM 和 HRTEM 照片

Fig. 3. TEM (a) and HRTEM (b) images of the as-prepared 5%In_2O_3/Ta_2O_5 composite.

均匀, 约为 240 nm, 具有明显的多孔结构; 而 In_2O_3 纳米粒子则分布在 Ta_2O_5 微球表面. 由样品的 HRTEM 照片可以清晰地观察到, In_2O_3 与 Ta_2O_5 之间存在着明显的界面, 且图片放大后的样品中晶面间距分别与正交晶相 Ta_2O_5 的 (010) 晶面和立方晶相 In_2O_3 的 (222) 晶面间距相吻合. 由此可见, In_2O_3 分布在多孔 Ta_2O_5 微球表面, 且两相间存在明显的界面.

2.2 In_2O_3/Ta_2O_5 的光吸收特性

图 4 为不同 In_2O_3 含量的 In_2O_3/Ta_2O_5 复合催化剂的 UV-Vis DRS 谱. 可以看出, 载体 Ta_2O_5 的吸收

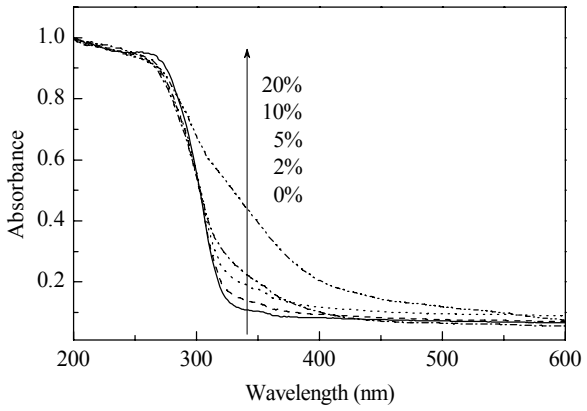

图 4 不同 In_2O_3 含量的 In_2O_3/Ta_2O_5 复合催化剂的紫外-可见漫反射光谱

Fig. 4. UV-Vis DRS of the as-prepared In_2O_3/Ta_2O_5 composites with different In_2O_3 mole percents.

带出现在 200~330 nm, 主要是由于 O 2*p* 轨道与 Ta 5*d* 轨道之间的荷移跃迁产生. 而 In_2O_3 的复合使得样品的光吸收带边明显红移到 450 nm, 这主要是 In 5*s*5*p* 轨道对带隙的贡献[15].

2.3 In_2O_3/Ta_2O_5 的光解水制氢活性

图 5 为不同 In_2O_3 含量 In_2O_3/Ta_2O_5 复合催化剂上模拟太阳光光解水制氢活性. 由图可见, 复合催化剂上产氢活性随着 In_2O_3 含量的增加而增加, 至 5% 时达最高, 为 78 μmol/h, 这可能是由于 In_2O_3 与 Ta_2O_5 复合形成的异质结构有利于光生电子与空穴的分离所致. 为了验证这一结论, 我们将 In_2O_3 与 Ta_2O_5 微球简单物理混合后制得 5%In_2O_3-95%Ta_2O_5 样品, 并在相同条件下进行测试. 结果发现, 其制氢

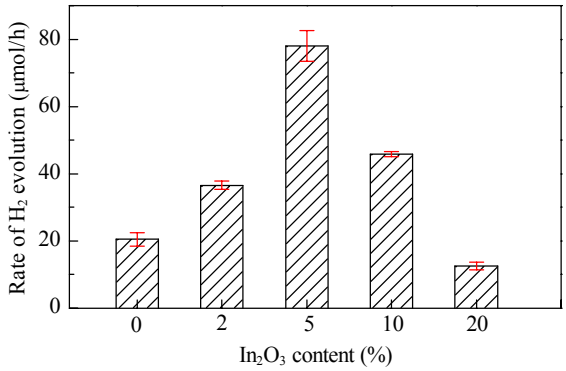

图 5 不同 In_2O_3 含量的 In_2O_3/Ta_2O_5 复合催化剂在模拟太阳光下的制氢活性

Fig. 5. Photocatalytic activity for hydrogen evolution of the as-prepared In_2O_3/Ta_2O_5 composites with different In_2O_3 mole percents under simulant solar light irradiation. Reaction conditions: reaction solution, 20 ml methanol + 80 ml water; catalyst amount, 0.15 g; Pt content, 1%; light source, 300 W Xe lamp; reaction time, 8 h.

活性仅为 28.9 μmol/h, 远低于复合材料. 这说明 In_2O_3/Ta_2O_5 异质结的形成在一定程度上实现了催化过程中光生电子与空穴的分离, 从而使复合材料表现出更高的光催化制氢活性. 由图 4 可见, In_2O_3/Ta_2O_5 复合材料的最大吸收带边约为 450 nm, 说明该材料可以对太阳光中部分可见光产生响应, 因此我们在模拟可见光源下, 考察了 5%In_2O_3/Ta_2O_5 上光催化制氢性能. 结果发现, 光照 8 h, 5%In_2O_3/Ta_2O_5 上可见光产氢速率只有 0.89 μmol/h, 这主要是由于 In_2O_3/Ta_2O_5 复合材料对光的吸收主要集中在 350 nm 以下, 因此可见光活性较低.

图 6 为 In_2O_3/Ta_2O_5 异质结在光催化过程中电荷分离示意图. In_2O_3 和 Ta_2O_5 的带隙分别为 2.8 和 4.0 eV, 二者导带均位于 H^+/H_2 还原电位之上, 分别为–0.62 和–0.17 V[16]. 在模拟太阳光照射下, In_2O_3 与 Ta_2O_5 会同时发生电子跃迁, 由于二者能带位置的差异, 电子从 In_2O_3 的导带迁移到 Ta_2O_5 的导带, 并发生还原反应产生氢气, 而空穴则由 Ta_2O_5 的价带迁移到 In_2O_3 的价带, 电荷的定向迁移实现了光生电子与空穴的分离, 从而提高了复合材料的产氢活性. 然而随着 In_2O_3 含量的进一步增加, 样品的产氢活性逐渐减低. 这是由于 In_2O_3 含量过高而在 Ta_2O_5 表面团聚, 且覆盖密度增加 (见图 1), 从而影响了光催化过程中光生电子与空穴的分离[17], 并减小了 Ta_2O_5 微球与反应液的接触面积与对光的吸收, 因而复合催化剂的产氢活性降低. 另一方面, 与我们前期制备的无定形介孔结构的 In_2O_3/Ta_2O_5 相比[18], 可分散的 In_2O_3/Ta_2O_5 异质结复合材料表现出明显更高的产氢活性, 这主要是由于可分散的 In_2O_3/Ta_2O_5 在保持一定的多孔性的同时, 具有较高

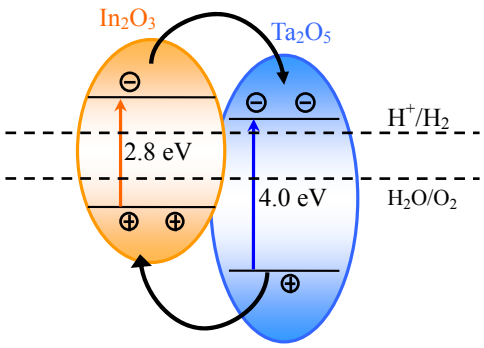

图 6 In_2O_3/Ta_2O_5 复合催化剂的电荷分离机理示意图

Fig. 6. Schematic illustration of the charge separation and transfer of as-prepared In_2O_3/Ta_2O_5 composites.

的结晶度与较好的分散性, 从而极大地改善了光生载流子在催化剂内部的迁移以及 In_2O_3 和 Ta_2O_5 与反应物的接触, 因此光催化产氢活性提高. 综上所述, 可分散的 In_2O_3/Ta_2O_5 复合光催化剂优异的产氢活性主要源于异质结有效的电荷分离作用以及复合材料较高的结晶度、较好的分散性和孔结构.

本文还考察了可分散的 5%In_2O_3/Ta_2O_5 复合光催化剂的稳定性, 每隔 8 h 对制氢系统抽真空, 重新进行模拟太阳光催化制氢实验, 循环 4 次, 结果示于图 7. 反应近 30 h 内复合材料的产氢速率无明显降低, 说明该催化剂在测试条件下具有较好的长效性.

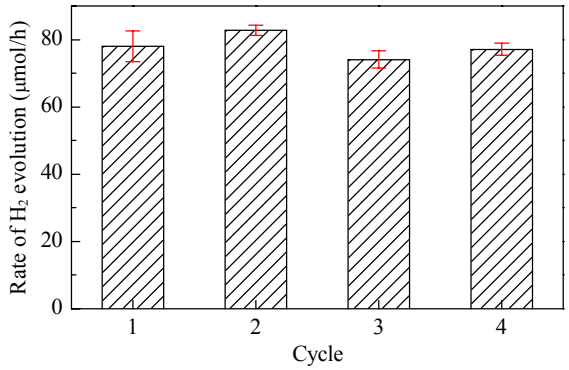

图 7 5%In_2O_3/Ta_2O_5 复合催化剂上模拟太阳光制氢稳定性

Fig. 7. Photocatalytic stabilities for hydrogen evolution of the as-prepared 5%In_2O_3/Ta_2O_5 composites under simulant solar light irradiation. Reaction conditions: reaction solution, 20 ml methanol + 80 ml water; catalyst amount, 0.15 g; Pt content, 1%; light source, 300 W Xe lamp; reaction time, 8 h.

3 结论

采用两步合成法制备了分散性较好的 In_2O_3/Ta_2O_5 异质结复合光催化剂, 并用于模拟太阳光催化制氢. 能带结构匹配的异质结的构建不仅可以拓宽半导体光响应范围, 还可有效地抑制光催化过程中光生电子与空穴的复合, 从而提高复合材料的光催化制氢活性. 同时, 异质结复合催化剂构型的优化与设计可以在一定程度上进一步促进界面电荷的分离, 有望在光催化制氢与环境净化等领域具有广泛的研究价值.

参 考 文 献

1 Chen X B, Shen S H, Guo L J, Mao S S. *Chem Rev*, 2010, **110**: 6503
2 Kitano M, Hara M. *J Mater Chem*, 2010, **20**: 627
3 马贵军, 雷志斌, 鄢洪建, 宗旭, 李灿. 催化学报 (Ma G J, Lei Zh B, Yan H J, Zong X, Li C. *Chin J Catal*), 2009, **30**: 73
4 黄翠英, 张澜萃, 李晓辉. 催化学报 (Huang C Y, Zhang L C, Li X H. *Chin J Catal*), 2008, **29**: 163
5 Kato H, Kudo A. *Chem Phys Lett*, 1998, **295**: 487
6 Osterloh F E. *Chem Mater*, 2008, **20**: 35
7 Takahara Y, Kondo J N, Takata T, Lu D L, Domen K. *Chem Mater*, 2001, **13**: 1194
8 Kondo J N, Uchida M, Nakajima K, Lu D L, Hara M, Domen K. *Chem Mater*, 2004, **16**: 4304
9 Yan H J, Yang J H, Ma G J, Wu G P, Zong X, Lei Z B, Shi J Y, Li C. *J Catal*, 2009, **266**: 165
10 Zong X, Yan H J, Wu G P, Ma G J, Wen F Y, Wang L, Li C. *J Am Chem Soc*, 2008, **130**: 7176
11 Wang X W, Liu G, Chen Z G, Li F, Wang L Z, Lu G Q, Cheng H M. *Chem Commun*, 2009: 3452
12 Wang Z Y, Huang B B, Dai Y, Qin X Y, Zhang X Y, Peng W, Liu H X, Yu J X. *J Phys Chem C*, 2009, **113**: 4612
13 Lü J, Kako T, Li Z S, Zou Z G, Ye J H. *J Phys Chem C*, 2010, **114**: 6157
14 Hisatomi T, Otani M, Nakajima K, Teramura K, Kako Y, Lu D L, Takata T, Kondo J N, Domen K. *Chem Mater*, 2010, **22**: 3854
15 Yang X, Wang Y H, Xu L L, Yu X D, Guo Y H. *J Phys Chem C*, 2008, **112**: 11481
16 Xu Y, Schoonen M A A. *American Mineralogist*, 2000, **85**: 543
17 刘阳, 王晟, 王鞠, 许章炼, 陈文兴, 蒋杰, 韦坚红. 催化学报 (Liu Y, Wang Sh, Wang T, Xu Zh L, Cheng W X, Jiang J, Wei J H. *Chin J Catal*), 2010, **31**: 485
18 Xu L L, Guan J G, Gao L, Sun Z G. *Catal Commun*, 2011, **12**: 548

英 译 文

English Text

Photocatalytic hydrogen production from water is an ideal technology for converting solar to chemical energy [1–4]. Ta-based materials consist of corner-sharing octahedral TaO_6, which is beneficial for the transfer of photogenerated electrons and holes. Moreover, the conduction band (CB) levels consist of Ta 5*d* orbit, which is much more negative than Ti 3*d* orbit, giving photogenerated electrons a strong reducing capability [5,6]. Hence, Ta-based materials attract considerable attention in the photocatalytic field of hydrogen production. However, the activation of UV light and co-catalyst requirements restrict practical applications of these materials [7,8]. Compared to ion doping and dye photosensitization, the fabrication of heterostructured composite semiconductor has advantages of effective photogenerated charge-carrier separation and optical response range extension. Heterostructured composites formed by simply mixing two kinds of semiconductors, such as Pt/PdS/CdS [9],

MoS_2/CdS [10], ZnO/CdS [11], ZnO/In_2O_3 [12], usually yield a small heterojunction area and complex photogenerated charge-carrier transfer to the surface, which limits light harvesting and reactant accessibility to active sites. Thus, the design and fabrication of heterostructured composites is important for the enhancement of photocatalytic activity for hydrogen production.

In this paper, on the basis of well-dispersed Ta_2O_5 microspheres, which are prepared using a mixture of tantalum ethoxide and glycolate as the precursor, dispersible heterostructured In_2O_3/Ta_2O_5 composites have been fabricated for photocatalytic hydrogen evolution under simulant solar light irradiation. We study the influence of In_2O_3 content on optical absorption properties and photocatalytic performance for hydrogen evolution, and propose a mechanism for photogenerated charge-carrier separation.

1 Experimental

1.1 Catalyst preparation

To prepare Ta_2O_5 microspheres, 0.4 g $Ta(OC_2H_5)_5$ was added to 10 ml ethylene glycol (in a glove box purged with nitrogen gas) and the solution was magnetically stirred for 8 h at room temperature to obtain a transparent solution. After removing the mixture from the glove box, it was immediately poured into an acetone bath (100 ml) containing 0.5 vol% of water, and stirred vigorously for 10 min. After aging for 30 min, the white precipitate was remove by centrifugation, followed by washing with deionized water and ethanol (three times), and then drying in a vacuum oven at 60 °C for 24 h to obtain well-dispersed Ta_2O_5 microspheres.

To prepare heterostructured In_2O_3/Ta_2O_5, 0.22 g of Ta_2O_5 microspheres were ultrasonically dispersed in 50 ml of water for 10 min. Then a certain amount of $In(NO_3)_3{\cdot}nH_2O$ were added while stirring at room temperature. To ensure complete precipitation, aqueous ammonia was subsequently added with constant stirring until pH > 9. Thereafter, the precipitates were separated by centrifugation, washed three times with deionized water and ethanol, and dried in an oven at 60 °C for 24 h subsequently. Finally, a white powder was obtained after annealing at 800 °C for 2 h.

1.2 Catalyst characterization

Scanning electron microscopy (SEM) images were recorded using a Hitachi S-4800 field-emission scanning electron microscope. Energy-dispersive X-ray (EDX) analyses were performed on a Horbia EX-250 energy-dispersive X-ray spectrometer. The crystalline structure of the samples was characterized with a D/Max-RB X-ray diffractometer (Rigaku, Tokyo, Japan, 0.05°/s scan rate, 15 kV accelerating voltage, 20 mA current, Cu K_α radiation, λ = 010154 nm). A JEM-100CXII electron microscope was used for both transmission electron microscopy (TEM) and high-resolution transmission electron microscopy (HRTEM) characterization. A UV-2550 UV-visible spectrophotometer (Shimadzu, Japan) was employed for UV-Vis diffuse reflectance measurements.

1.3 Photocatalytic test

The photocatalytic activity of the samples for hydrogen evolution was studied in a LabSolar H_2 closed-gas circulation system connected to a gas chromatograph. A PLS-SXE300 xenon lamp with IR filter (300 W, 320 nm < λ < 780 nm) was used as the simulant solar light source, a PLS-SXE300 xenon lamp with a UV-cut filter was employed as the visible light source. The catalyst (150 mg) and chloroplatinic acid (3.15 mg, 1 wt%) was added to a quartz glass vessel, containing 80 ml deionized water and 20 ml methanol, and this was connected to a closed gas circulation system. Stirring uniformly disperses the mixtures. An in situ photodeposition method was used to load Pt onto the as-prepared photocatalysts [13,14]. Before irradiation, the closed system was repeatedly evacuated to –0.1 MPa to remove dissolved oxygen and other gases. Thereafter, the connection between the vacuum pump and circulation system was closed and the suspension was irradiated. After a given interval of irradiation, in-situ analyses of constant volume gases were performed using a gas chromatograph (GC 7890-II, Shanghai TECHCOMP Co. Ltd.) with MS-5A molecular sieve column, 45 °C column temperature, nitrogen carrier, and a thermal conductivity detector. The injection and detection temperatures are both 120 °C, and the current is 100 mA.

2 Results and discussion

2.1 Structural and morphological characterizations of In_2O_3/Ta_2O_5 composites

Figure 1 shows the SEM images and EDX spectra of the as-prepared In_2O_3/Ta_2O_5 composites with different In_2O_3 contents. It can be seen that the Ta_2O_5 microsphere morphologies are well remained during the preparation process, with an average diameter of about 240 nm. After calcination, the microsphere becomes rough with increased surface defects. The In species mainly exist on the surface of support and aggregate with increasing In content. The corresponding EDX spectra show that all composites consist of Ta, O, and In elements.

Figure 2 shows the XRD patterns of the as-prepared In_2O_3/Ta_2O_5 composites. All samples display characteristic dif-

fraction peaks of orthorhombic Ta_2O_5 (JCPDS 79-1375) at 2θ = 23.1°, 29.2°, 37.8°, 47.3°, 51.2°, and 56.8°. With increasing In_2O_3 content to 20%, the characteristic diffraction peaks at 2θ = 30.6° and 35.5° correspond to the cubic phase of In_2O_3 (JCPDS 71-2194), indicating the existence of In_2O_3 in the as-prepared composites. With increasing In_2O_3 content the intensity of Ta_2O_5 diffraction peaks decreases, suggesting that introducing In_2O_3 has a negative effect on Ta_2O_5 crystallinity.

Figure 3 displays the TEM and HRTEM images of the as-prepared 5%In_2O_3/Ta_2O_5 composite. The well-dispersed Ta_2O_5 microspheres exhibit obvious porous structure with an average diameter of about 240 nm. In_2O_3 nanoparticles distribute on the surface of Ta_2O_5 microspheres. As shown in the HRTEM image, there is an obvious interface between In_2O_3 and Ta_2O_5. We index the interplanar spacing from the magnified image to (010) planes of the orthorhombic Ta_2O_5 phase and (222) facets of the cubic In_2O_3 phase. The results indicate that In_2O_3 composites distribute on the surface of porous Ta_2O_5 microspheres with a clear interface between the two phases.

2.2 Optical absorption properties of In_2O_3/Ta_2O_5 composites

Figure 4 shows the UV-Vis DRS for the as-prepared In_2O_3/Ta_2O_5 composites with different In_2O_3 contents. The Ta_2O_5 support absorption band appears at 200–330 nm indicating charge transfer from O 2*p* orbitals to Ta 5*d* orbitals. After In_2O_3 incorporation, the composite absorption band edges show an obvious red shift at approximately 450 nm, because of In 5*s*5*p* orbit contribution to the band gap [15].

2.3 Photocatalytic water splitting for hydrogen production of In_2O_3/Ta_2O_5 composites

Figure 5 displays photocatalytic water splitting for hydrogen evolution of the as-prepared composites with different In_2O_3 contents under simulant solar light irradiation. We perform photocatalytic tests in a methanol aqueous solution under irradiation (300 W Xe lamp) for 8 h. With an increase in In_2O_3 content, we observe an increase in photocatalytic activity of the as-prepared composite, where 5%In_2O_3/Ta_2O_5 exhibits the highest hydrogen evolution rate of 78 μmol/h. We attribute this increase in photocatalytic activity to heterostructure formation between In_2O_3 and Ta_2O_5, which is beneficial for photogenerated charge-carrier separation, and results in enhanced photocatalytic activity of the composites. To confirm the former, we prepared the 5%In_2O_3-95%Ta_2O_5 sample by mechanically mixing In_2O_3 and Ta_2O_5 microspheres. The photocatalytic activity of the sample is only 28.9 μmol/h evaluated under the same conditions, which is much less than as-prepared composites, indicating that heterostructure formation between In_2O_3 and Ta_2O_5 causes the photogenerated charge-carrier separation, resulting in enhanced photocatalytic activity for hydrogen evolution. Figure 4 clearly shows that the In_2O_3/Ta_2O_5 composite absorption band edge onset is about 450 nm, indicating response to the visible part of solar light. We also study visible light photocatalytic activity of 5%In_2O_3/Ta_2O_5 under simulant visible light irradiation. After irradiation for 8 h, the hydrogen evolution rate is only 0.89 μmol/h. This is due to limited absorption under 350 nm, resulting in lower visible light photocatalytic activity.

Figure 6 shows a schematic illustration of charge separation of as-prepared In_2O_3/Ta_2O_5 composites. The band gaps of In_2O_3 and Ta_2O_5 are 2.8 and 4.0 eV, respectively, and correspond to CBs of –0.62 and –0.17 V, respectively [16], which is more negative than the H^+/H_2 reduction potential. Under simulant solar light irradiation, electron transitions occur simultaneously in both In_2O_3 and Ta_2O_5. Because of different energy band positions, photoexcited electrons transfer from the In_2O_3 CB to that of Ta_2O_5 to produce hydrogen, while holes transfer from the valence band of Ta_2O_5 to that of In_2O_3. Directional charge transfer achieves separation of photogenerated electrons and holes, thus enhancing photocatalytic activity for hydrogen production. We attribute decreasing photocatalytic activity with increasing In_2O_3 content to the aggregation of superfluous In_2O_3 nanoparticles on the surface of Ta_2O_5 microspheres (Fig. 1). This process not only restrains the separation of photogenerated electrons and holes, but also decreases the contact area between Ta_2O_5 microspheres and the reactant, resulting in the decreased photocatalytic activity. On the other hand, compared to amorphous mesoporous In_2O_3/Ta_2O_5 prepared by our group [18], the well-dispersed heterostructured In_2O_3/Ta_2O_5 composite exhibits an enhanced photocatalytic activity because of porosity, high crystallinity, and good dispersity. The latter properties greatly improve the transfer of photogenerated charge carriers in the In_2O_3/Ta_2O_5 composite and photocatalyst-reactant contact, thus enhancing photocatalytic activity for hydrogen evolution. To sum up, we attribute the enhanced photocatalytic activity of the well-dispersed In_2O_3/Ta_2O_5 composite to heterostructure (causing efficient charge separation) as well as high crystallinity, good dispersity, and porous structure.

We evaluate the stability of the well-dispersed 5%In_2O_3/Ta_2O_5 composite photocatalyst. We evacuate the closed gas circulation system under vacuum each 8 h and repeat the photocatalytic test four times. Figure 7 shows that there is no noticeable decrease in photocatalytic hydrogen evolution rates within 30 h, suggesting satisfactory long-term effects of the as-prepared composite under the present reaction conditions.

3 Conclusions

Well-dispersed heterostructured In_2O_3/Ta_2O_5 composite photocatalysts were prepared using a two-step synthesis method for photocatalytic hydrogen evolution under simulant solar light irradiation. The fabrication of heterojunctions with appropriate energy band structures, not only extends the optical absorption of the semiconductors, but also efficiently restrains the recombination of photogenerated electrons and holes, thus enhancing photocatalytic activity for hydrogen evolution. Hence, the design and optimization of the heterojunction morphology facilitates the separation of interfacial charges, and benefits the development of highly efficient photocatalytic materials in hydrogen evolution and environmental purification fields.

Full-text paper available online at Elsevier ScienceDirect
http://www.sciencedirect.com/science/journal/18722067